LAWRENCE
LIVERMORE
NATIONAL
LABORATORY

UCRL-TR-237273

900-24 Mock Tensile Tests

B. J. Cunningham, F. J. Gagliardi

December 14, 2007

Disclaimer

This work performed under the auspices of the U.S. Department of Energy by Lawrence Livermore National Laboratory under Contract DE-AC52-07NA27344.

Test Series Description

In September of 2007, LLNL received 55 mock tensile specimens that had been machined to standard tensile specimen geometry (see Figure 1). All specimens received were tested, in tension, with the exception of a single specimen from hemisphere 1 that had arrived broken. Tests were conducted at several temperatures and strain rates using the standard LLNL tensile test fixture mounted in the MTS 858 hydraulic test frame (see Figure 2). Strain was measured using a pair of 0.5-inch gage-length Shepic extensometers equipped with V knives. Each test was conducted using Flextest GT Control Software at nominal strain rates of 0.0001/s or 0.1/s. Rates were controlled in real time using feedback from the average of the two gages. Tests were performed at several temperatures including -54 ± 0.5˚C, room temperature (23.5 +0.5/-0.0˚C), and 74˚C ± 0.5˚C.

Test Methodologies

Heating and cooling ramp rates were no greater, on average, than 1˚C per minute and all specimens were allowed to soak at the target test temperature for a minimum of 15 minutes prior to test initiation. All test samples were lubricated at the cone ends using a Dow 33 low-temperature lubricant. Prior to testing, the extensometers were calibrated using a Boeckeler digital micrometer and determined to be within 2% accuracy over a 10,000-microstrain range. The MTS load cell was checked against a NIST-traceable Transducer Techniques® load cell and found to be in agreement with the standard to better than 1-pound. Tests were conducted according to the LANL-supplied test plan shown in Table 1.

Specimen Identification

Specimens were delivered as individually unlabeled parts grouped by hemispherical pressing number, 01 to 04, and separated as either P (pole) or E (equator) samples. An identification number was added to each sample prior to testing. A typical identification sequence would be, for example, 01-4E, indicating that it was taken from hemisphere 1, was number four in sequence, with an extraction region and orientation of type E.

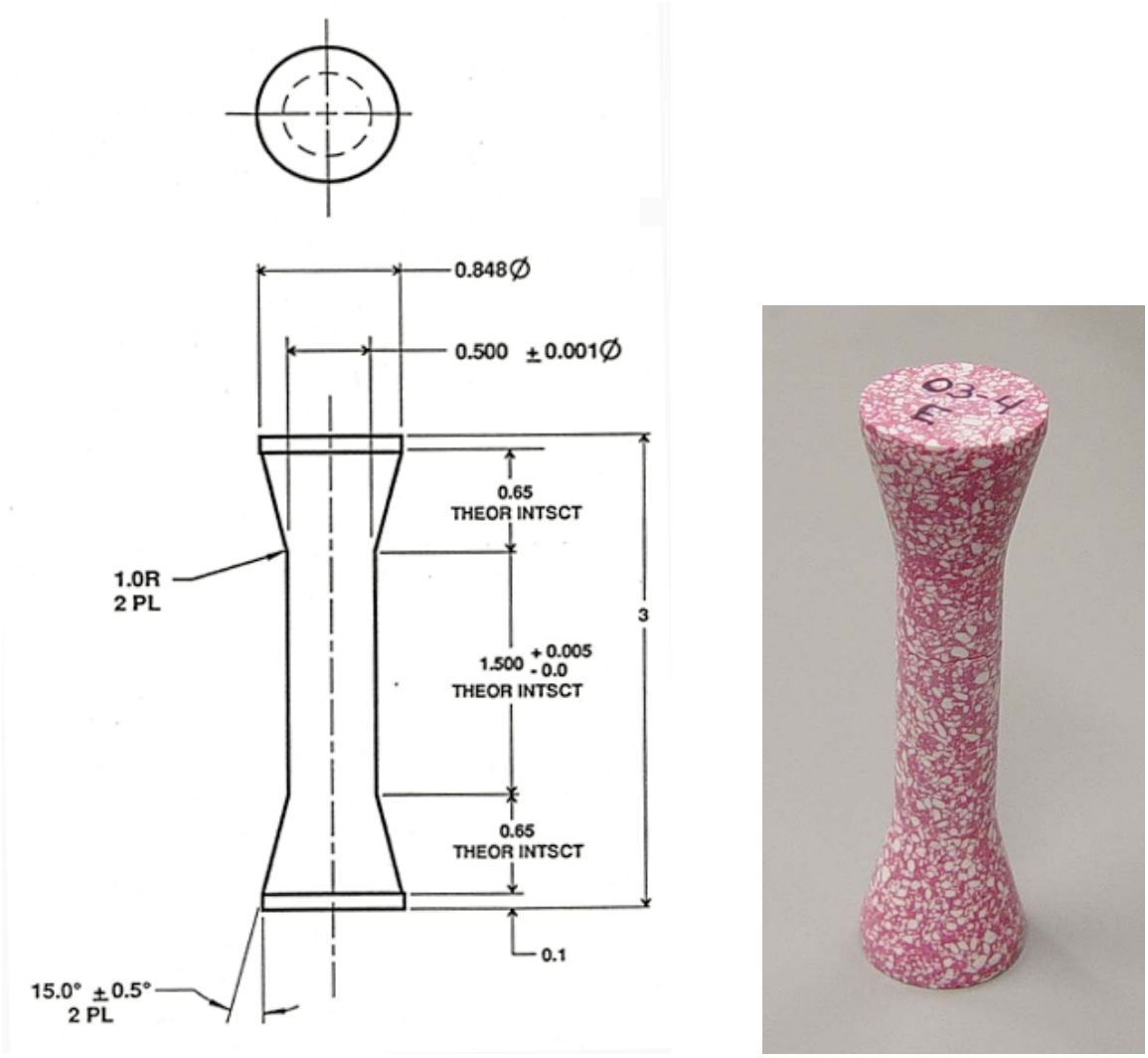

Figure 1 – Tensile specimens used in this study were machined according to the standard geometric specifications used in surveillance tests, displayed in the drawing on the left. A representative sample of Mock 900-24 is shown on the right. In the drawing, units are in inches. In the photo, white regions are cyanuric acid, pink regions are a mixture of talc, Kel-F 800™, and red die.

Figure 2 – Tensile tests were conducted using the standard LLNL tensile fixture mounted in an MTS 858 hydraulic test unit. An MTS model 651.05 environmental chamber was used to control test temperatures at -54˚C, room temperature, and 74˚C. Liquid nitrogen was used to cool the specimens and resistance coils were used to supply heat.

Table 1. Mock 900-24 Tensile Test Plan

Sample Location	Number of Samples	Test Temp (deg C)	Strain Rate (1/s)	
Inert - 1				
F: 47475-02, 03-A39325-0002				
Equator	2	-54	slow	
(axial)	2	20	slow	
	2	74	slow	
	2	-54	fast	
	2	20	fast	
	1	20	slow	(spare, test if available)
Pole	1	20	slow	
(hoop)	1	-54	slow	
	1	20	fast	
A: 47475-04, 03-A39325-0004				
Equator	2	-54	slow	
(axial)	2	20	slow	
	2	74	slow	
	2	20	fast	
	2	74	fast	
	2	20	slow	(spare, test if available)
Pole	1	20	slow	
(hoop)	1	74	slow	
	1	74	fast	
Inert-2				
F: 47475-01, 03-A39325-0001				
Equator	2	-54	slow	
(axial)	2	20	slow	
	2	74	slow	
	2	-54	fast	
	2	20	fast	
	1	20	slow	(spare, test if available)
Pole	1	20	slow	
(hoop)	1	-54	slow	
	1	-54	fast	
A: 47475-03, 03-A39325-0003				
Equator	2	-54	slow	
(axial)	2	20	slow	
	2	74	slow	
	2	20	fast	
	2	74	fast	
	1	20	slow	(spare, test if available)
Pole (hoop)	1	-54	fast	

Strain Rate definition:
slow - consistent with Pantex surveillance testing (~1e-4/sec)
fast - as fast as feasible up to 1/sec

Note: The room temperature tests were conducted, not at 20˚C as shown, but at 23.5 +0.5/-0.0˚C, to facilitate comparisons with PBX 9502 data. The high rate used was nominally 0.1/s.

Prior to each test, the specimen's length and shank diameter were measured using a digital micrometer. During each test, the following values were recorded:

1) Time (seconds)
2) Stroke (inches)
3) Load (pounds)
4) Engineering Strain, Extensometer 1 (microstrain)
5) Engineering Strain, Extensometer 2 (microstrain)
6) Extensometer Average = (Ext. 1 + Ext. 2) / 2
7) Engineering Stress = Load / Specimen area based on the initial diameter of shank

Following some of the tests, low magnification images of the specimen fracture surfaces were generated (see Appendix A). For each test, plots of strain data from the two extensometers, as well as linear fits to the strain-time curves were made to determine strain rates, and to look for evidence of extreme bending.

Data and Data Analysis

Subsequent to our first 900-24 test (an 04 specimen test performed at 0.0001/s and room temperature), a stress-strain plot of the data was made, along with representative curves generated from previously tested RM-03-AC mock data (see Figure 3). This was done to provide some early perspective on 900-24 performance relative to similar, previously tested mocks. All plots are of the actual data. The RM-03-AC tests had also been performed at room temperature and 0.0001/s. RM-03-AC mock is identical in constituent mix ratios to 900-24 (60.9% talc, 24.1% talc, and 15% Kel-F 800™). The two previously tested mocks are identified in the plot as RM-03-AC Batch #1 and Batch #2. Also plotted is data from a typical virgin PBX 9502 specimen (Lot 890-010) tested at room temperature and at a strain rate of 0.0001/s. As may be seen, the three mocks differ significantly in both stress and strain-at-failure, in spite of the fact that their constituents are virtually identical. The reason for the differences is that for plastic bonded explosives and explosive mocks, material behavior depends on many factors beside the constituent recipe. Some of the additional factors include:

1) The exact form of each constituent –for example the talc particle size and shape (see Appendix D).

2) The manner in which the materials were combined (the manner of "mixing").
3) The process used to compact the material (was it die, billet, or hemi pressed?).
4) The temperature at which the material was pressed.
5) The pressing pressure.
6) The number and duration of the pressing cycles.
7) The materials post-pressing mechanical and thermal history. For example, thermal cycling or exposure to stress can alter a material behavior.

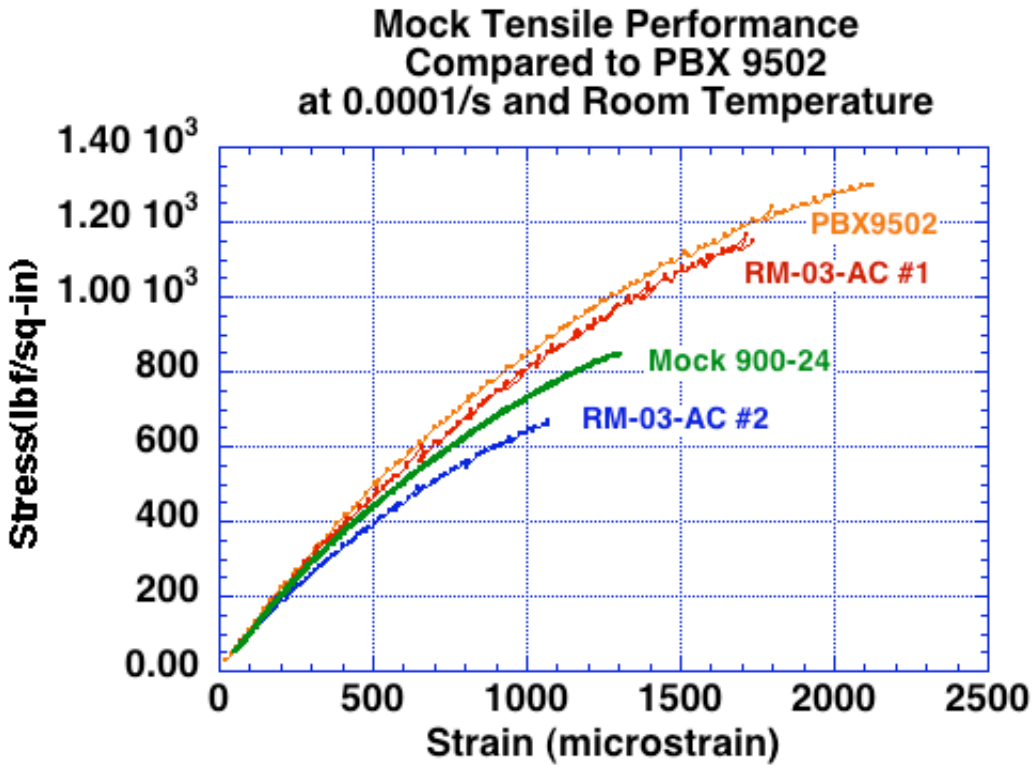

Figure 3 – First-test comparison of mock 900-24 with data from previously tested, same-constituent mocks at 0.0001/s and room temperature. Note that the 900-24 specimen falls between the two RM-03-AC mocks in the amount of stiffness (overall curve slope), ultimate stress, and strain at ultimate stress that it exhibits. Also note that all mock specimens display lower performance, relative to PBX 9502, based on the metrics of stress and strain at fracture.

Comparing the curves, we see that the 900-24 data falls between the two RM-03-AC mocks in regard to strength and strain-at-failure. All the mock

specimens may be seen to exhibit less ultimate stress and strain-at-failure than is exhibited by the PBX 9502 specimen.

Figure 4 shows fracture surfaces from the two types of RM-03-AC mock tensile samples, as well as a fracture surface from a representative PBX 9502 tensile specimen. Also shown is the failure surface from the 900-24 04-12E specimen whose data is shown in Figure 1. In these photomicrographs, we see that the failure surface of the PBX 9502 specimen is relatively flat with the failure surfaces for the RM-03-AC specimens slightly less so. In contrast, the fracture surface of the 900-24 specimen is the most heavily contoured. In the case of the 900-24 specimen, failure paths appear to have been influenced by inhomogeneities in the material. The white particle

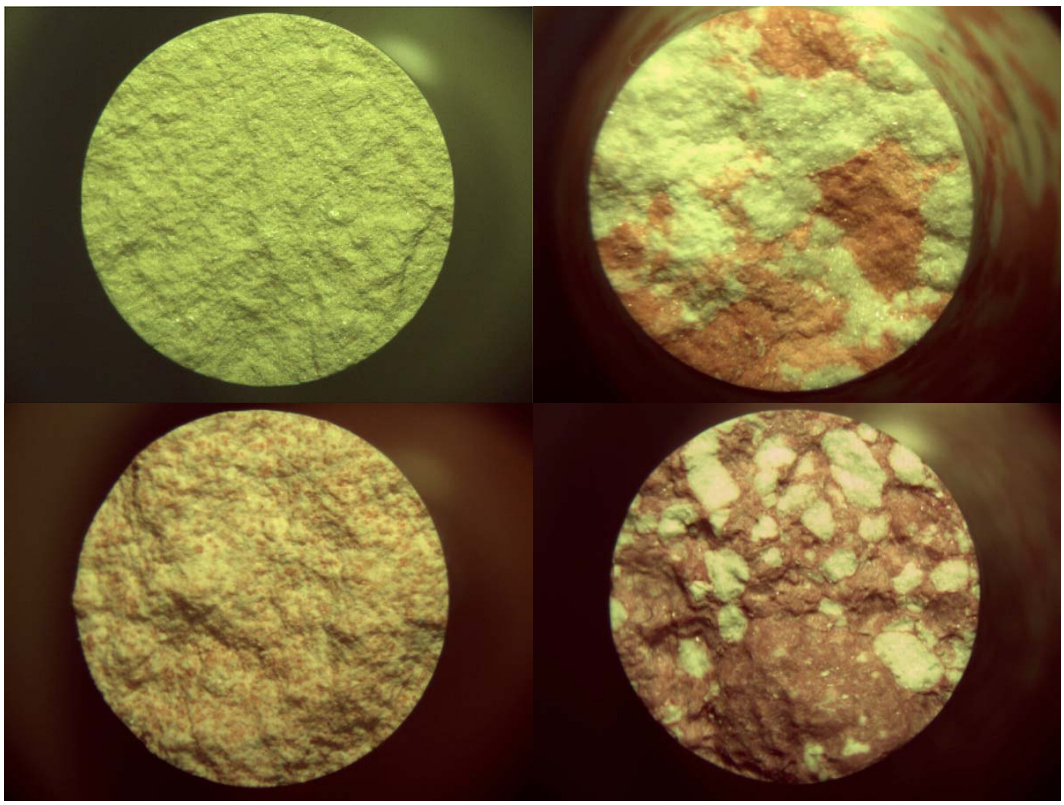

Figure 4 – Photomicrographs of four tensile specimen fracture surfaces. Clockwise from top left is PBX 9502, RM-03-AC #1, 900-24, and RM-03-AC #2.

conglomerates are cyanuric acid, while the pink material is a mixture of talc and Kel-F 800™. The talc-Kel-F 800™ matrix appears to exhibit regions of

relative weakness (note the large, pink convex area at the bottom of the fracture surface). We note that a lack of material homogeneity could be the source of anomalous behavior, such as early part failure. Figure 5 shows a top and side view of a 900-24 fracture surface emphasizing the uneven nature of the breakage.

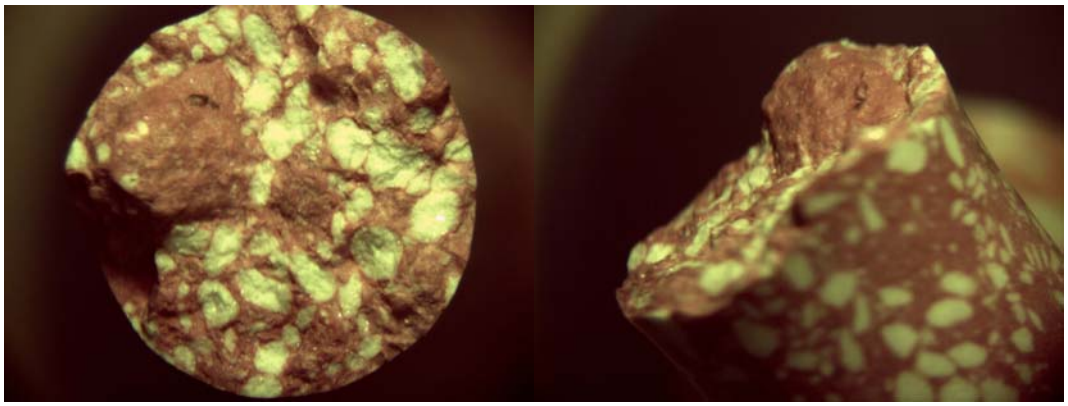

Figure 5 – Post-test photomicrographs of a tensile specimen shown from two angles. The side view emphasizes the irregular fracture surface exhibited by many of the 900-24 tensile specimens. The uneven failure surface is thought to be associated with inhomogeneities in material strength that could result in anomalous behavior, such as early breakage.

We observed that parameters for the four source pressings were listed in the pressing sheets attached to the specimen shipment. These pressing sheets indicate that all of the hemispheres used to generate parts were pressed at a temperature of 90˚C, and a pressure of 15,000-psi, using a single cycle with a 5-minute dwell time. These parameters, relative to what we would normally use when pressing a TATB-based PBX, are fairly low. We performed a physical density measurement on a cylindrical section removed from the 900-24 sample that was received broken (the water solubility of the cyanuric acid precludes immersion density measurements). The density, based on the section's weight and geometry, was found to be1.886 g/cc. This density is consistent with what would be expected for a PBX 9502 density mock. Appendix E contains results from a study using LANL-supplied mock powder to examine the effect of pressing temperature on compression behavior of this 900-24 mock.

Figures 6 and 7 show overlays of typical 900-24 data selected from tests covering the spectrum of nominal strain rates and test temperatures. From these plots, we can see that, as we would expect, the material generally becomes stiffer (has a higher average curve slope) as temperatures decrease and as strain-rate increases. The material also shows an increasing strain-at-failure with increasing temperature. In addition, it exhibits greater strain at failure at the higher rate when warm than it does at the lower rate.

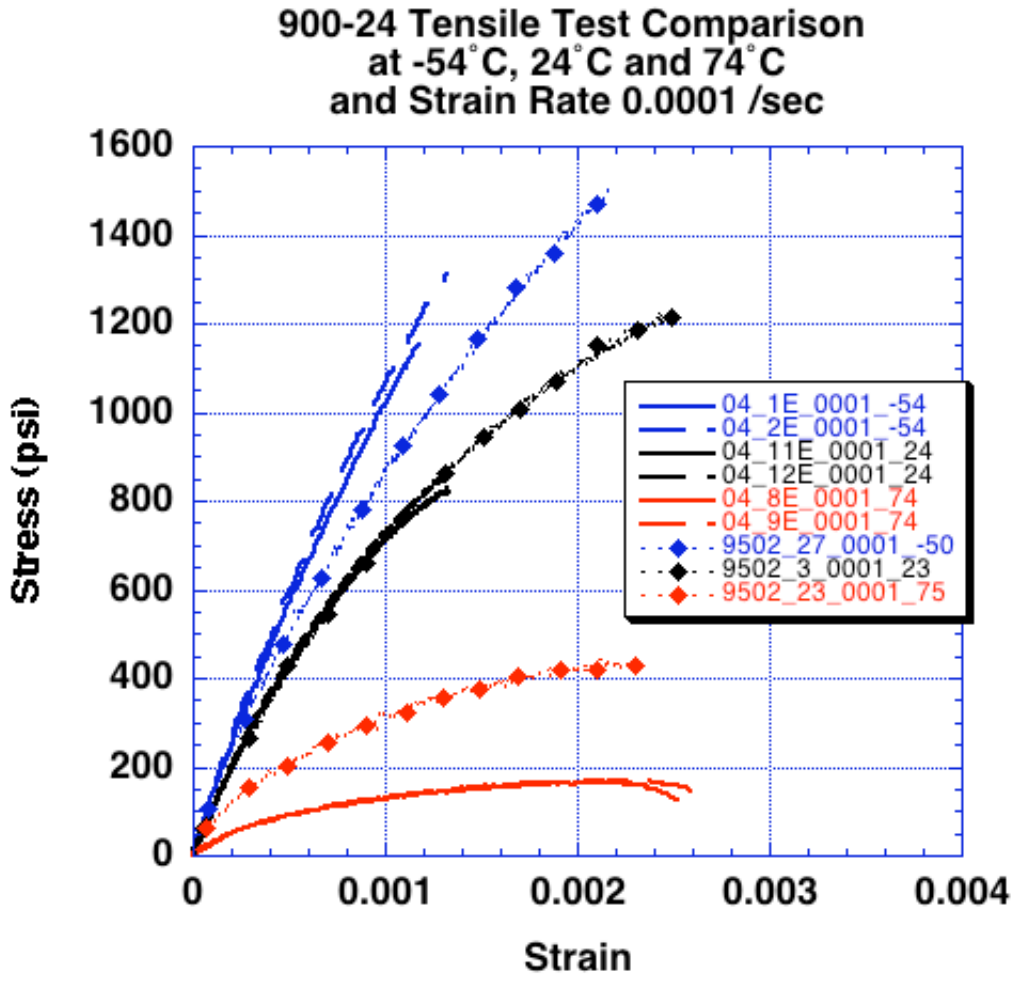

Figure 6 – Comparison plot of tensile behavior of mock 900-24 and PBX 9502 at -54˚C, 24˚C, and 74˚C and strain rate of 0.0001/sec. The stiffness and the strength of the mock material can be seen to have an inverse relationship with test temperature. PBX 9502 has greater ultimate strength in all cases.

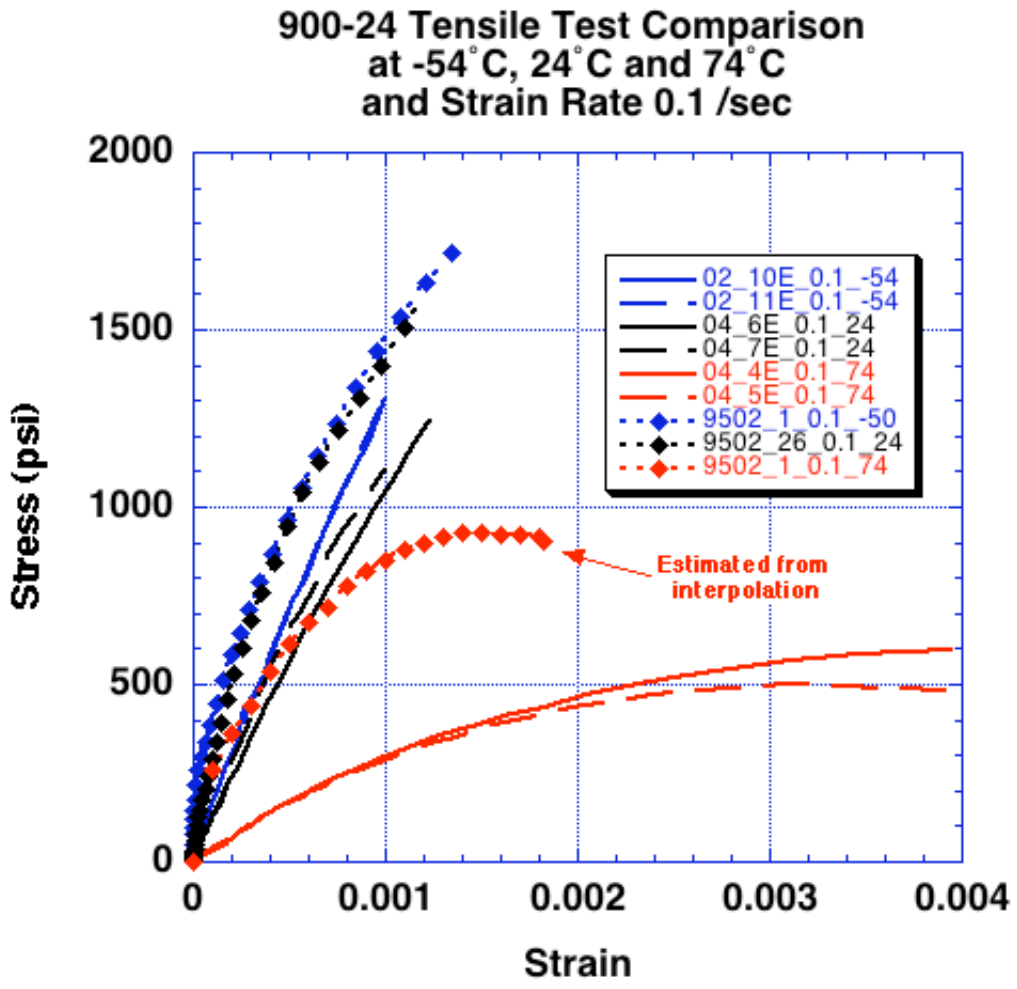

Figure 7 – A comparison of the tensile behavior of mock 900-24 and PBX 9502 at -54˚C, 24˚C, and 74˚C and strain rate of 0.1/s. Hemispherical pressings 02 and 04 are shown here as examples. At the strain-rate of 0.1/s the ambient and cold tests show similar stiffness and ultimate strength, whereas at the lower rate of 0.0001/s the cold data was noticeably stiffer and stronger. Like the slower strain rate data, the PBX 9502 shows greater ultimate strength at all test temperatures.

Appendix B lists individual test results, by specimen, giving both maximum stress and strain-at-maximum-stress. In the case where there were two tests for the same hemi pressing at the same temperature and strain rate, results are averaged, and the variation between tests were noted. Exact details may be obtained by reading the table. Figures 8 through 13 plot data by strain

rate and temperature. Hemispheres 02 and 04 produced samples that generally out-performed those from hemispheres 01 and 03. This difference is most easily seen in the high temperature data, but the ordering is also present, to some degree, in the room temperature and cold slower rate data as well. At the high rate and cold temperature, the 02 hemi is seen to exhibit greater strain at failure than does the 01, while the ultimate strengths for the 01 and 02 pressings, at these test conditions, were approximately the same.

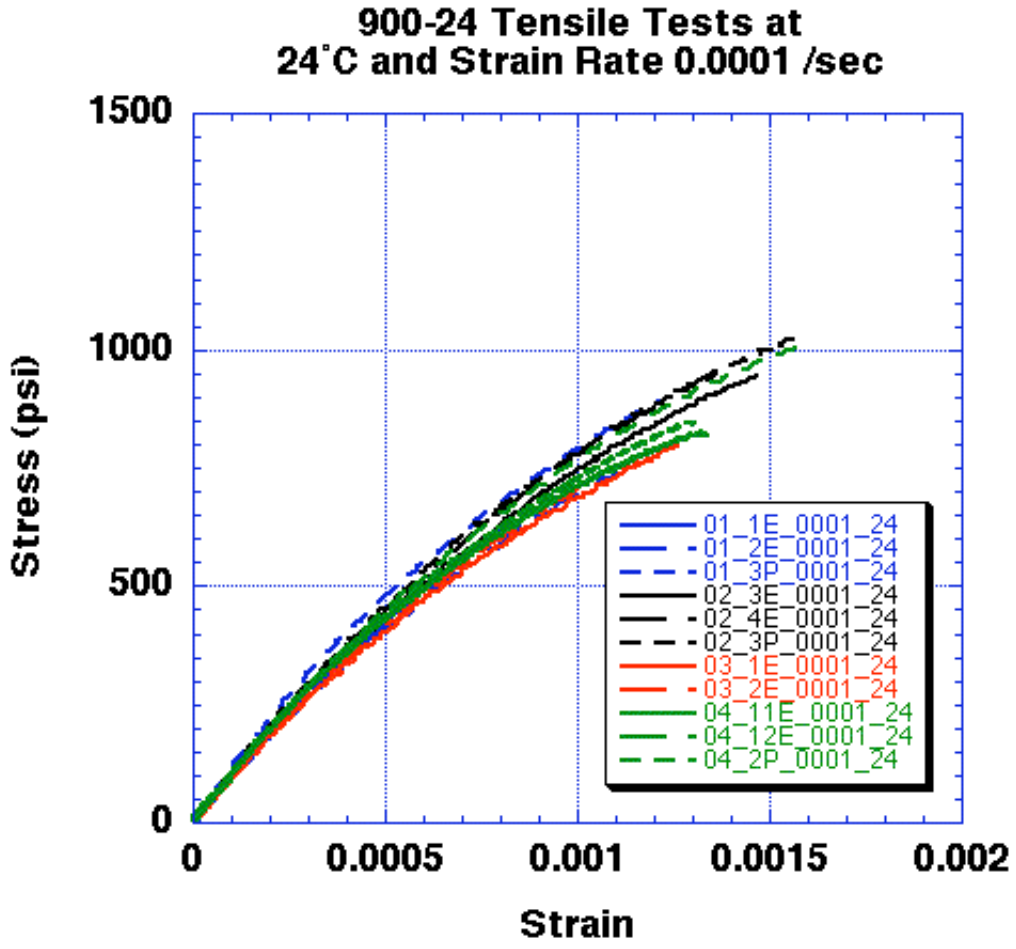

Figure 8 – Comparison of all four of the hemispherical pressings' tensile data at room temperature and a strain rate of 0.0001/sec.

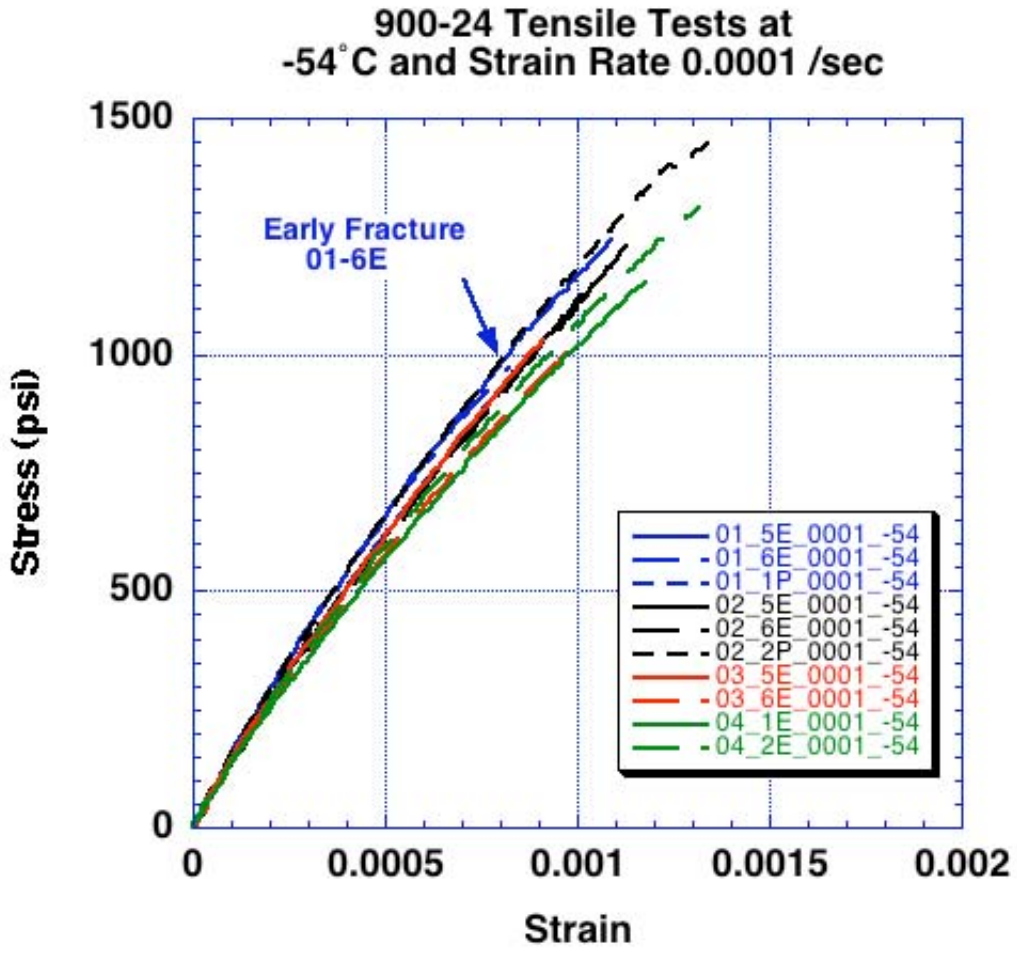

Figure 9 – Comparison of all four of the hemispherical pressings' tensile data at -54˚C and a strain rate of 0.0001/sec. Sample 6E from hemi 01 broke early.

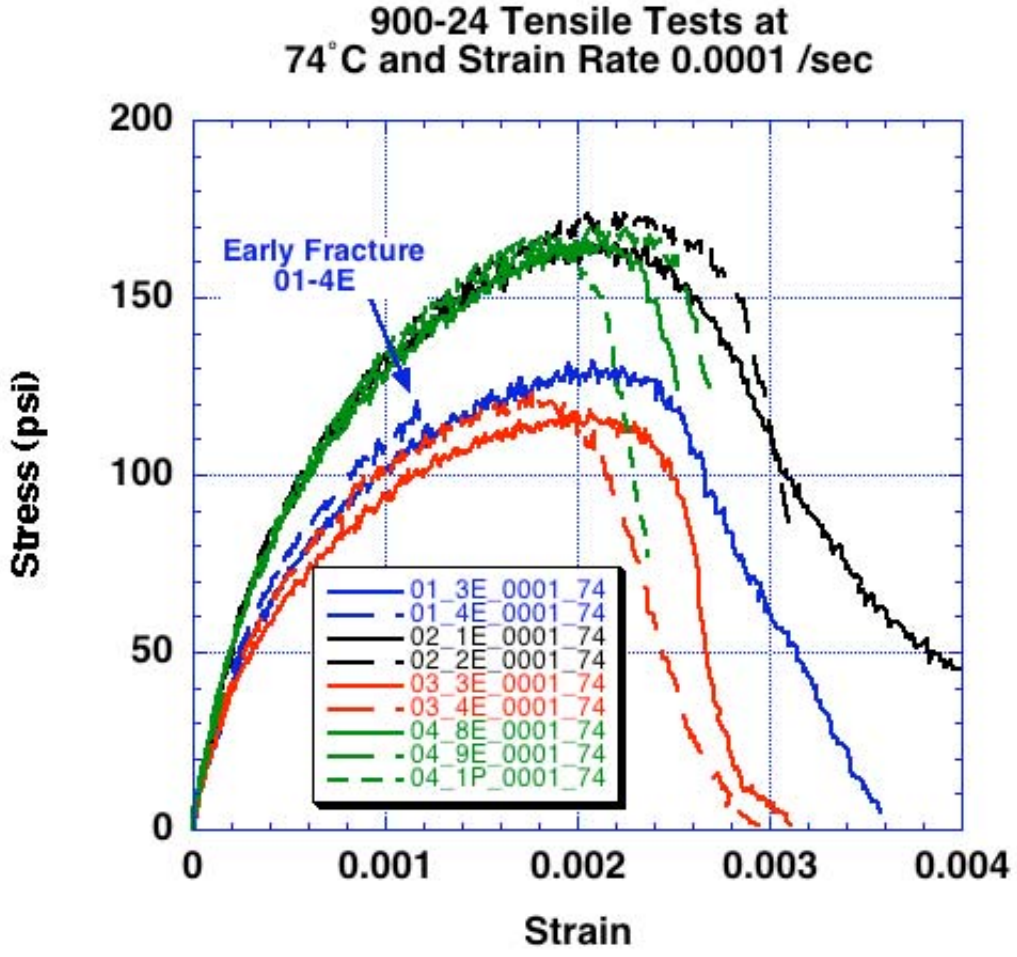

Figure 10 – Comparison of all four of the hemispherical pressings' tensile data at 74˚C and a strain rate of 0.0001/sec. Sample 4E from hemi 01 showed early fracture. Hemis 02 and 04 showed greater performance than did hemispheres 01 and 03.

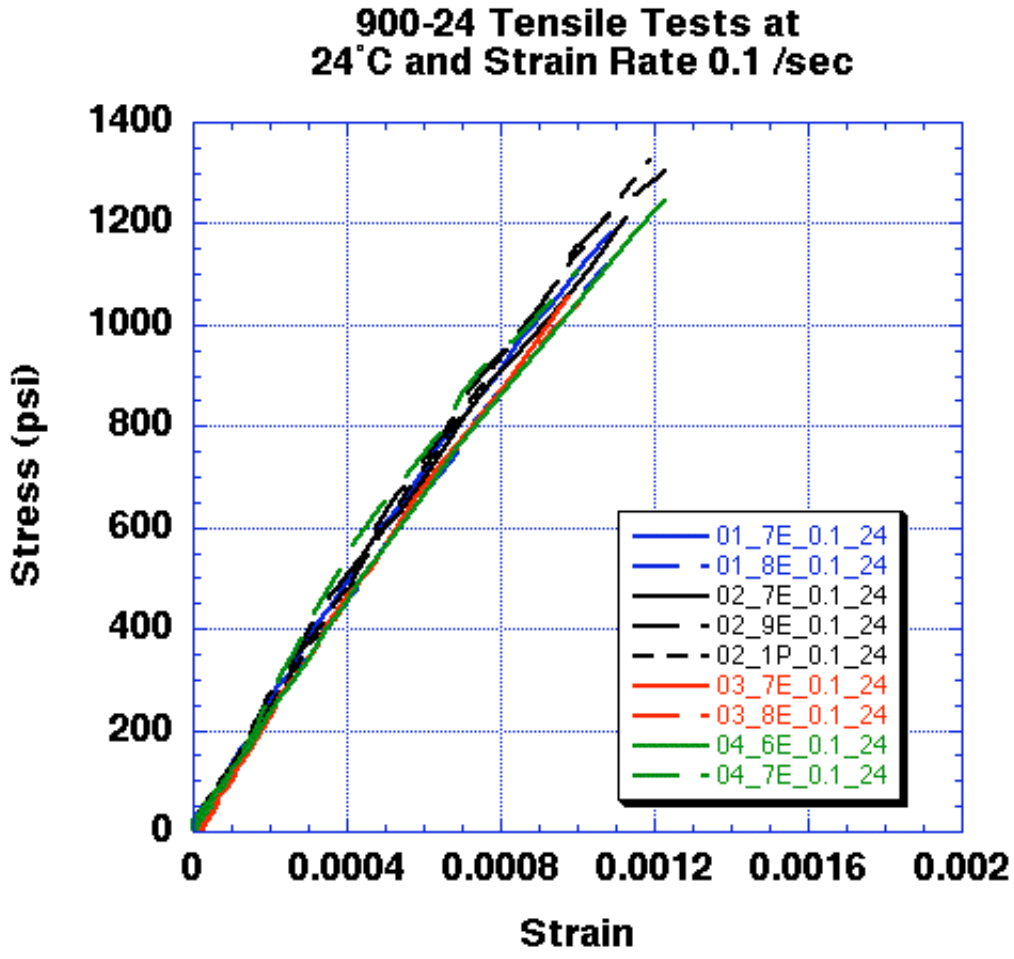

Figure 11 – Comparison of all four of the hemispherical pressings' tensile data at room temperature and a strain rate of 0.1/sec.

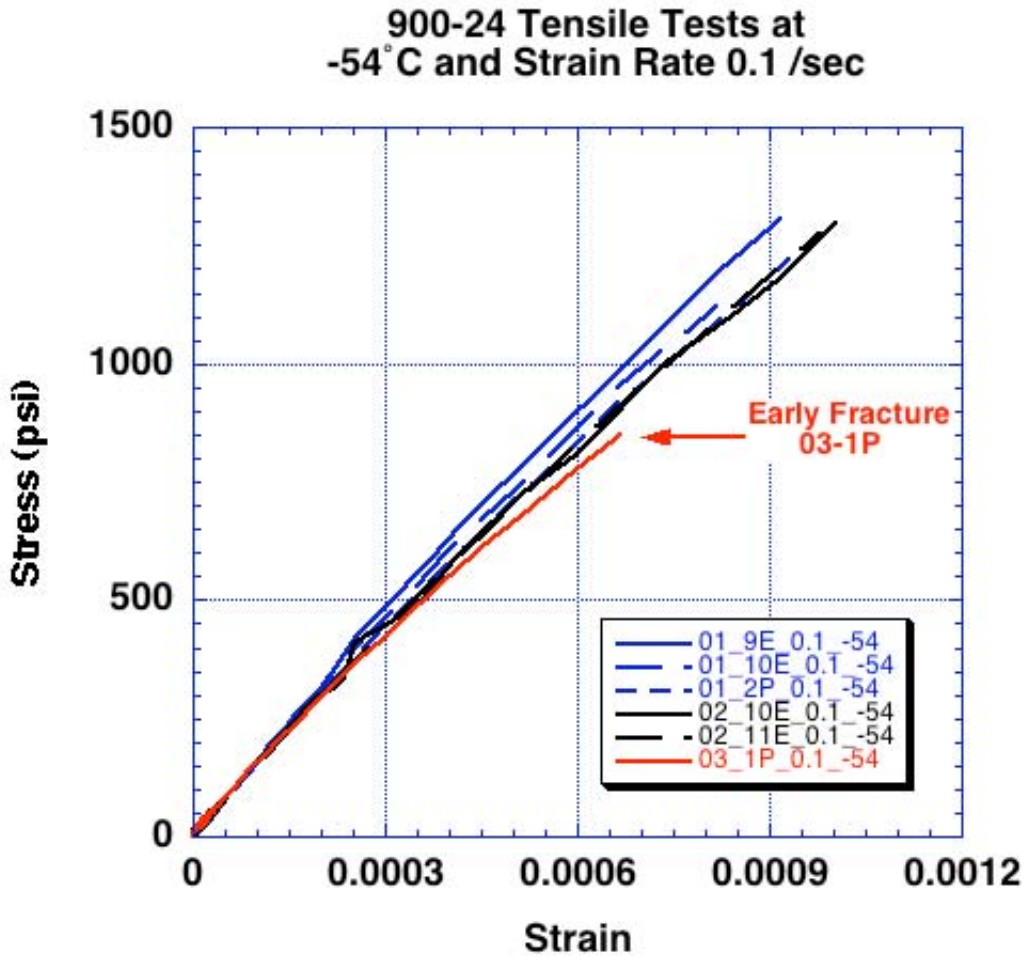

Figure 12 – Comparison of three of the hemispherical pressings' tensile data at -54˚C and a strain rate of 0.1/sec.

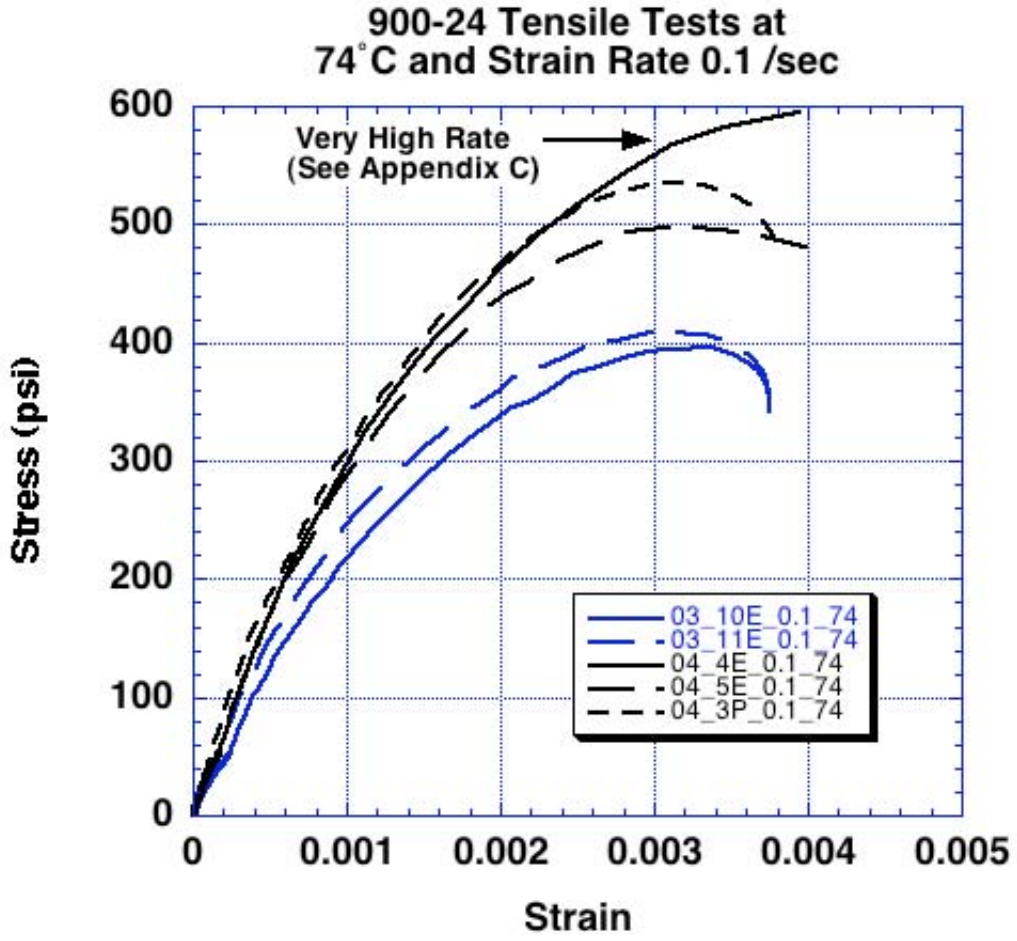

Figure 13 – Comparison of two of the hemispherical pressings' tensile data at 74˚C and a strain rate of 0.1/sec. Sample 04-4E was inadvertently tested at a relatively high strain-rate resulting in a noticeably higher ultimate stress.

Comparing "P" specimen performance to that of "E" specimens, "P" specimens exhibited, overall, slightly greater ultimate stress and strain-at-failure at room temperature than did the "E" specimens. Neither appeared to exhibit an advantage at the high temperature. It is unclear whether the "P" specimens possess any advantage at cold temperatures. In making these observations, it is important to recognize the fact that there was a very limited number of "P" specimens from which to draw conclusions.

In a few of the tests (03-1P, 01-6E, and 01-4E) failures appear to have occurred early, possibly due to localized bonding problems that may have

caused regions of weakness. Data from anomalous tests of this type are not indicative of nominal behavior. These tests do, however, suggest that there may be regions of weakness within the pressings that may serve as sights for fracture origination.

Notes on Data Acquisition and Control Issues

Because the material being tested is relatively weak, it demonstrates comparatively little stress and strain-at-failure. This results in raw data that appears somewhat noisy due to the short plotting range, especially in the case of data taken from tests performed at elevated temperatures. Because the noise is relatively high frequency it does not significantly affect the underlying curve shapes.

Achieving controlled high strain-rates in tests such as these is difficult, since acceleration of the physical components involved is limited by inertial effects. This means that, when testing at high rates, the best one can do is to program the system to achieve an approximately correct strain rate at the time of sample failure. The tests performed in this series were the first high strain-rate tests performed on our MTS 858 system. Consequently, trial and error for each temperature-rate combination was necessary in order to arrive at the test parameters that would produce a smooth ramp up to near the desired rate. A discussion of rate effects on ultimate stress, with specific reference to this data, is presented in Appendix C.

In a few instances, a slight waviness may be observed in the high-rate plots. This waviness is the consequence of the system making rapid control adjustments as it attempts to arrive at specified rate. Again, this behavior should have had only a small affect on the data.

Finally, we are currently limited in our system to a maximum acquisition rate of 1024-Hz. This creates an uncertainty in strain-at-failure for some of our high-rate tests of approximately 50-microstrain. Because of the way the material fails at high-temperature (failure occurs past the peak), this uncertainty applies only to the data from the high-rate cold and room temperature tests. These tests should be adjusted by extrapolating the curves' end points and noting the uncertainties.

Appendix A

Fracture Surfaces

900-24 Arrived Broke#89BE...

900-24 Arrived Broke#89BE...

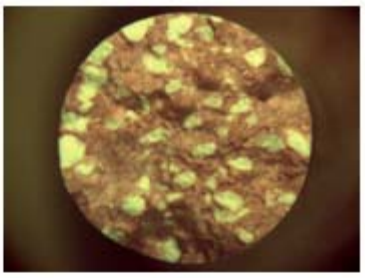

900-24a_01_2E0001_74.jpg

900-24a_01_3E_0001_74.jpg

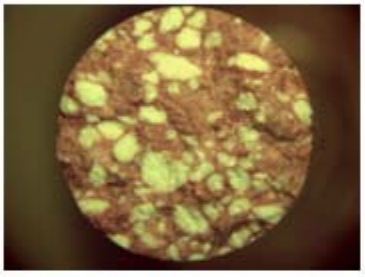

900-24a_02_3P_0001_24.jpg

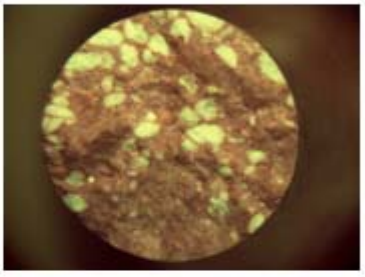

900-24a_02_6E_0001_-54.jpg

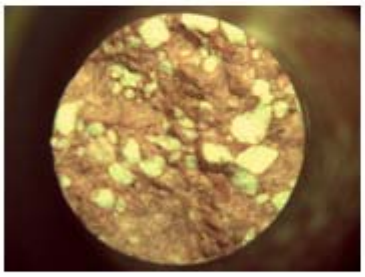

900-24a_02_7E_pt1_24.jpg

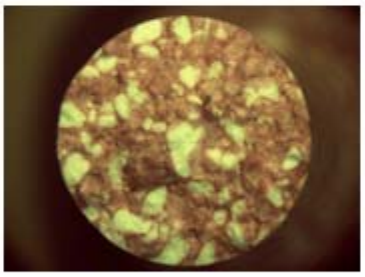

900-24a_03_1E_0001_24.jpg

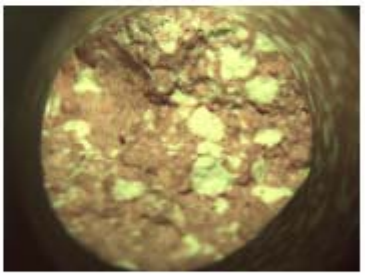

900-24a_03_9E_pt1_74.jpg

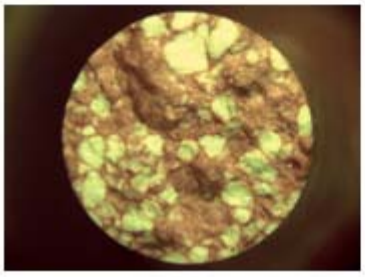

900-24a_04_2E.jpg

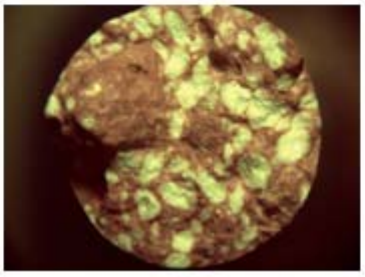

900-24B_02_4E_0001_24.jpg

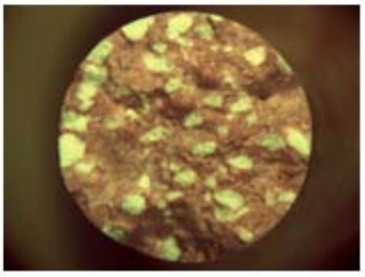

900-24b_01_2E_0001_74.jpg

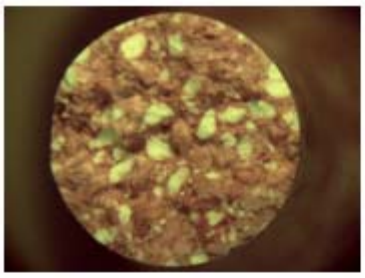

900-24b_01_3E0001_74.jpg

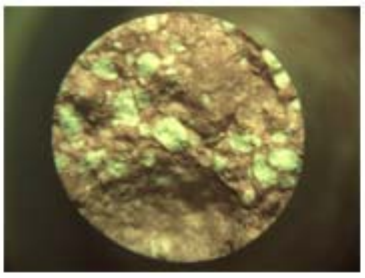

900-24b_02_2P_0001_-54.jpg

900-24b_02_3P_0001_24.jpg

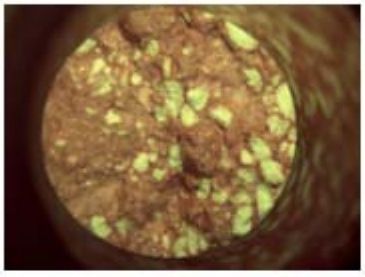

900-24b_02_6E_0001_-54.jpg

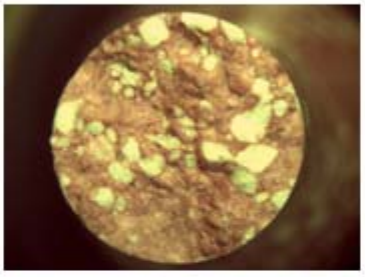

900-24b_02_7E_pt1_24.jpg

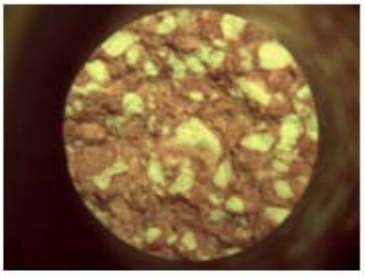

900-24b_03_1E_0001_24.jpg

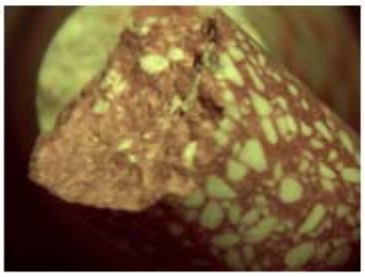

900-24b_03_3E_0001_7#89B...

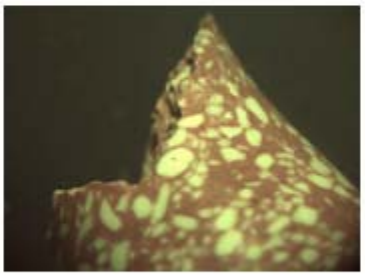

900-24b_03_9E_pt1_74.jpg

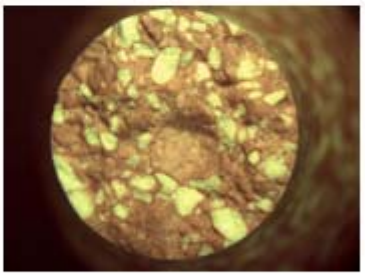

900-24b_04_1E_0001_-54.jpg

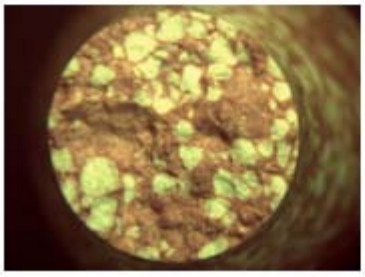

900-24b_04_2E.jpg

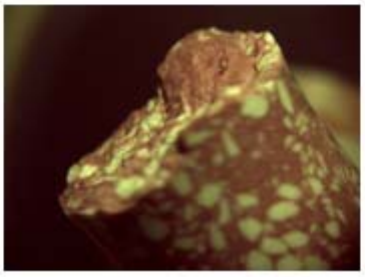

900-24C_02_4E_0001_24.jpg

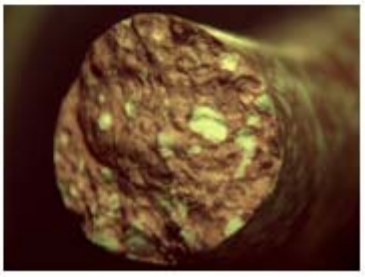

900-24c_03_3E_0001_2#89B...

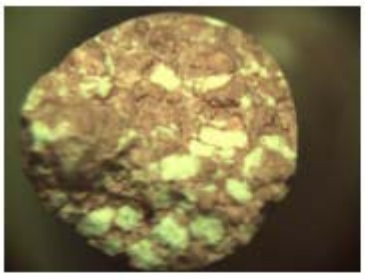

900-24c_03_9E_pt1_74.jpg

900-24_01_1E_0001_24.jpg

900-24_01_3Pb_0001_24.jpg

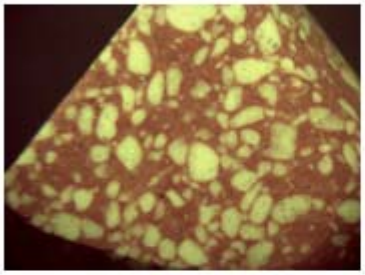

900-24_01_3Pc_flat on end.jpg

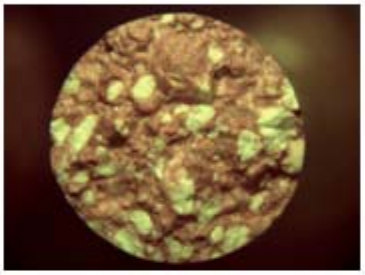

900-24_01_3P_0001_24.jpg

900-24_01_4E_0001_74#89B...

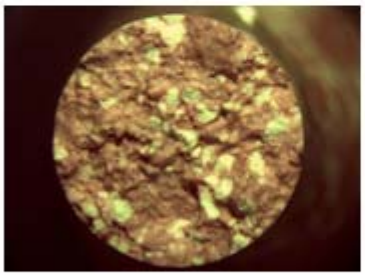

900-24_02_2E_0001_74#89B...

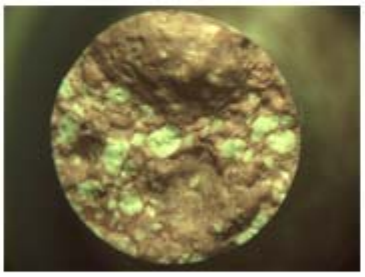

900-24_02_2P_0001_-54.jpg

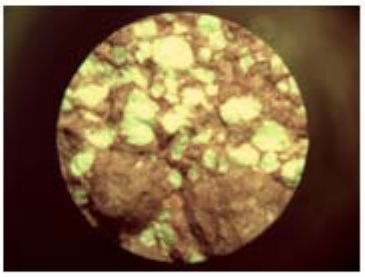

900-24_02_3E.jpg

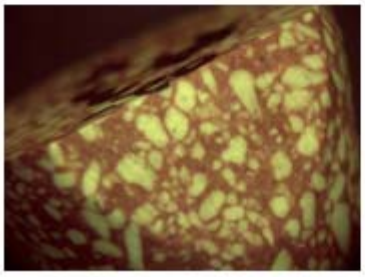

900-24_02_3P_0001_24_flat.jpg

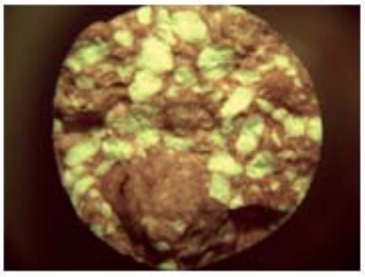

900-24_02_4E_0001_24.jpg

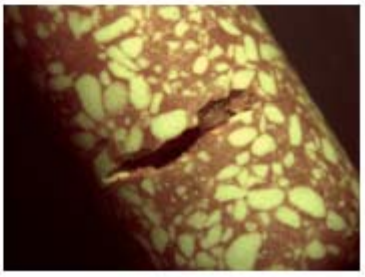

900-24_02_5E_chip out.jpg

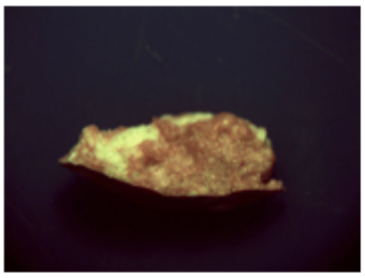

900-24_02_5E_chip.jpg

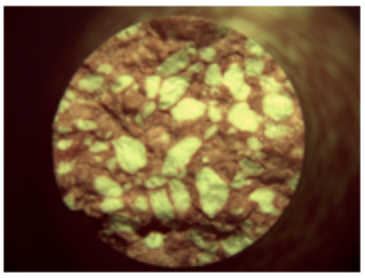

900-24_02_5E_top view.jpg

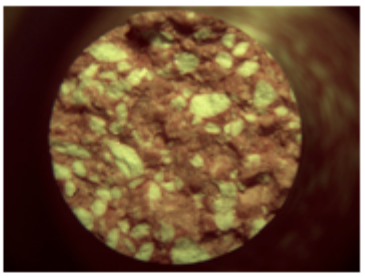

900-24_03_2E_0001_24.jpg

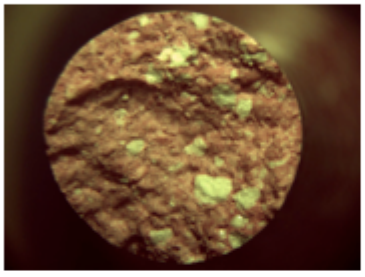

900-24_03_3E_0001_74.jpg

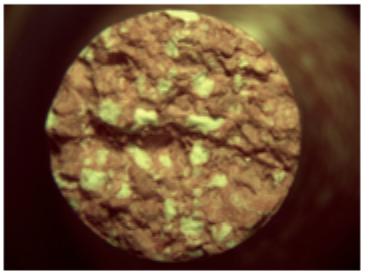

900-24_03_4E_0001_74#89B...

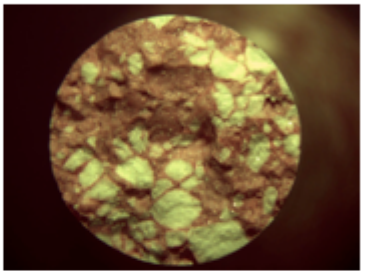

900-24_04_10Eb_pt1_24.jpg

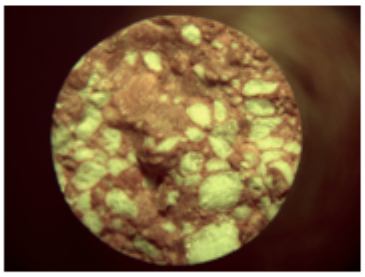

900-24_04_10E_pt1_24.jpg

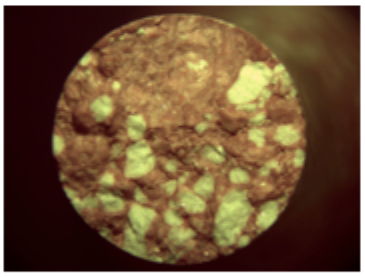

900-24_04_11Eb_0001_24.jpg

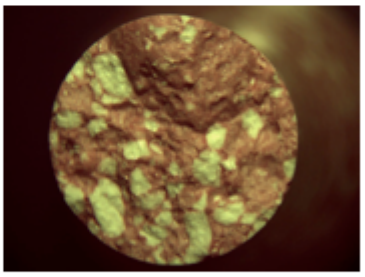

900-24_04_11E_0001_24.jpg

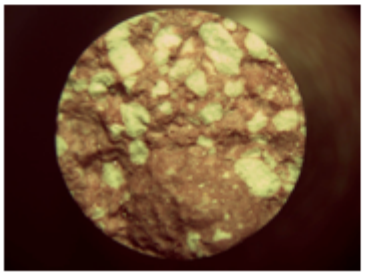

900-24_04_12E_weak r#89B...

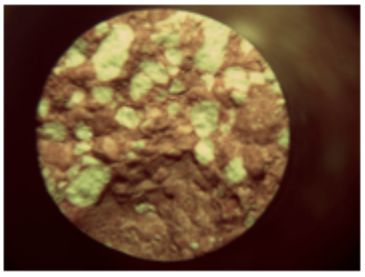

900-24_04_12E_weak region....

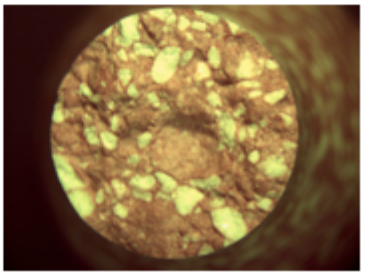

900-24_04_1E_0001_-54.jpg

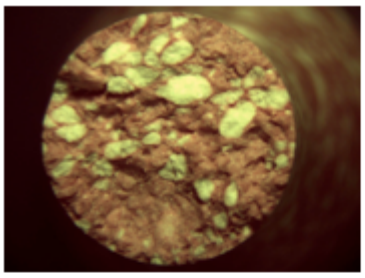

900-24_04_1P_0001_74#89...

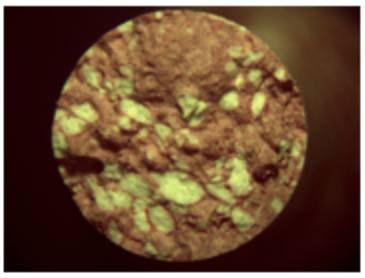

900-24_04_1P_0001_74#89...

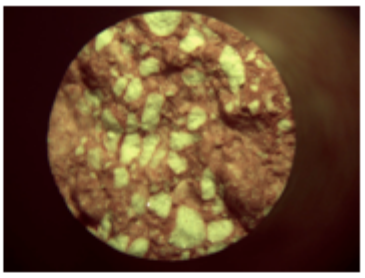

900-24_04_2P_0001_24#89...

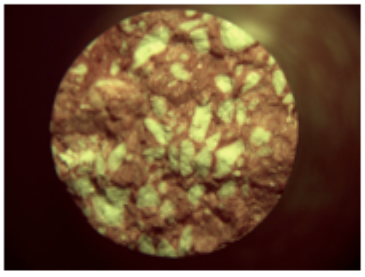

900-24_04_2P_0001_24#89...

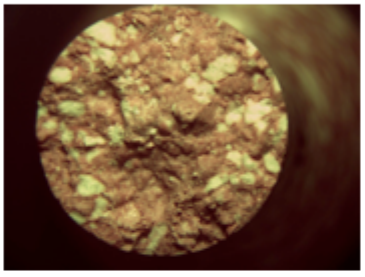

900-24_04_8E_0001_74_1.jpg

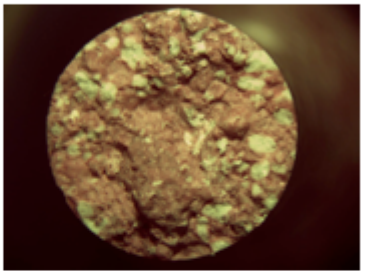

900-24_04_8E_0001_74_2.jpg

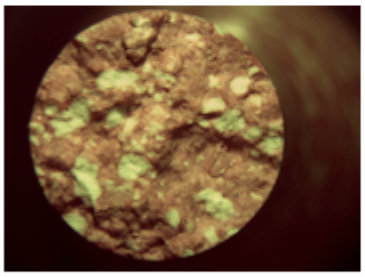

900-24_04_9E_2_bead pullo...

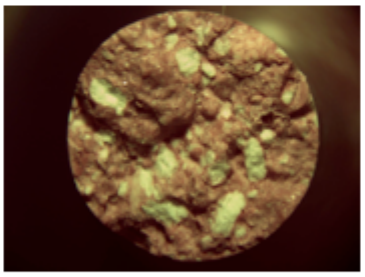

900-24_04_9E_bead pullout.jpg

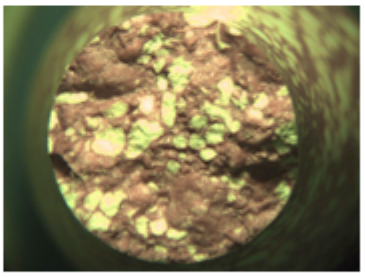

900_24_01_6E_0001_-54.jpg

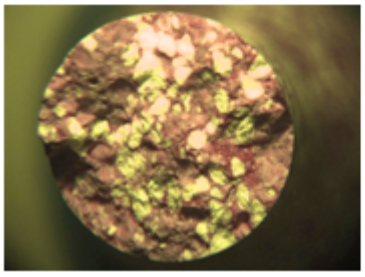

900_24_03_1P_pt1_-54.jpg

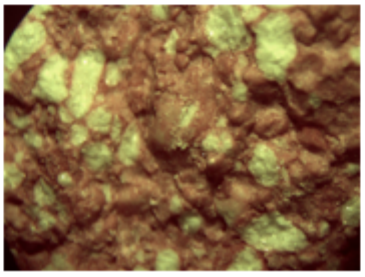

Arrived broken surfa#89BE4...

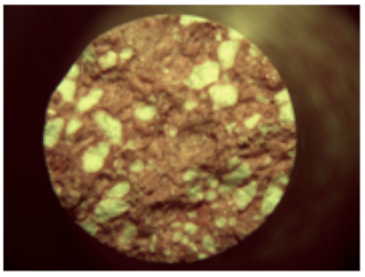

Arrived broken surfa#89BE4...

Appendix B

Data

Hemi	Sample #	Position	Temp. (˚C)	Strain Rate	Ult. Stress	Strain at Ult. Stress	Avg. stress	+ or -	Avg. Strain	+ or -	% Spread Stress	% Spread Strain
1	5	E	-54	0.0001	1242	1089	1108.5	133.5	955	134	12.04	14.03
1	6	E	-54	0.0001	975	821						
1	1	P	-54	0.0001	990	871	-	-	-	-	-	-
1	2	P	-54	0.01	1277	985	-	-	-	-	-	-
1	9	E	-54	0.1	1305	918	1212.5	92.5	867	51	7.63	5.88
1	10	E	-54	0.1	1120	816						
1	1	E	24	0.0001	641	860	692	51	981	121	7.37	12.33
1	2	E	24	0.0001	743	1102						
1	3	P	24	0.0001	892	1212	-	-	-	-	-	-
1	7	E	24	0.1	1183	1090	1150	92	1083	7	8.00	0.65
1	8	E	24	0.1	1117	1076						
1	3	E	74	0.0001	129	2078	123	6	1621	457	4.88	28.19
1	4	E	74	0.0001	117	1164						

Hemi	Sample #	Position	Temp. (˚C)	Strain Rate	Ult. Stress	Strain at Ult. Stress	Avg. stress	+ or -	Avg. Strain	+ or -	% Spread Stress	% Spread Strain
2	5	E	-54	0.0001	1231	1127	1178.5	52.5	1075.5	51.5	4.45	4.79
2	6	E	-54	0.0001	1126	1024						
2	2	P	-54	0.0001	1448	1353	-	-	-	-	-	-
2	10	E	-54	0.1	1300	1004	1287.5	12.5	989	15	0.97	1.52
2	11	E	-54	0.1	1275	974						
2	3	E	24	0.0001	944	1469	947	3	1410	59	0.32	4.18
2	4	E	24	0.0001	950	1351						
2	3	P	24	0.0001	1021	1574	-	-	-	-	-	-
2	7	E	24	0.1	1211	1130	1254	43	1173	43	3.43	3.67
2	9	E	24	0.1	1297	1216						
2	1	P	24	0.1	1324	1190	-	-	-	-	-	-
2	1	E	74	0.0001	164	2179	168	4	2193.5	14.5	2.38	0.66
2	2	E	74	0.0001	172	2208						

Hemi	Sample #	Position	Temp. (˚C)	Strain Rate	Ult. Stress	Strain at Ult. Stress	Avg. stress	+ or -	Avg. Strain	+ or -	% Spread Stress	% Spread Strain
3	5	E	-54	0.0001	1032	916	1034	2	962.5	46.5	0.19	4.83
3	6	E	-54	0.0001	1036	1009						
3	1	P	-54	0.1	850	668	-	-	-	-	Early Failure	
3	1	E	24	0.0001	795	1260	792	3	1230.5	29.5	0.38	2.40
3	2	E	24	0.0001	789	1201						
3	7	E	24	0.1	1057	977	1062	5	1007.5	30.5	0.47	3.03
3	8	E	24	0.1	1067	1038						
3	3	E	74	0.0001	116	2062	118.5	2.5	1949	113	2.11	5.80
3	4	E	74	0.0001	121	1836						
3	10	E	74	0.1	409	3030	402.5	6.5	3197	167	1.61	5.22
3	11	E	74	0.1	396	3364						

Hemi	Sample #	Position	Temp. (˚C)	Strain Rate	Ult. Stress	Strain at Ult. Stress	Avg. stress	+ or -	Avg. Strain	+ or -	% Spread Stress	% Spread Strain
4	1	E	-54	0.0001	1155	1178	1231	76	1245.5	67.5	-6.17	5.42
4	2	E	-54	0.0001	1307	1313						
4	11	E	24	0.0001	822	1332	835	13	1316.5	15.5	-1.56	1.18
4	12	E	24	0.0001	848	1301						
4	2	P	24	0.0001	1010	1606	-	-	-	-	-	-
4	6	E	24	0.1	1244	1230	1172	72	1111.5	118.5	6.14	10.66
4	7	E	24	0.1	1100	993						
4	8	E	74	0.0001	165	2116	166.5	1.5	2167	51	-0.90	2.35
4	9	E	74	0.0001	168	2218						
4	1	P	74	0.0001	166	1842	-	-	-	-	-	-
4	4	E	74	0.1	595	3940	547	48	3536.5	403.5	8.78	11.41
4	5	E	74	0.1	499	3133						
4	3	P	74	0.1	536	3222	-	-	-	-	-	-

Appendix C

Rate Effects

Under “Notes on Data Acquisition and Control Issues”, several problems with achieving target strain rates were mentioned. In particular, it was noted that, for high-rate tests of the type performed on our hydraulic system, a constant rate is generally not achievable and that the best we can expect is to program the system so that the sample is experiencing approximately the target strain rate at time of failure. Since the system programming required to achieve this condition varies with the material, the strain-rate and the temperature, high rate testing is subject to rate errors. The problem is especially acute if the material being tested fails at low strains, since the time the system is given to achieve the desired condition is minimized.

Given the fact that, at high rates, rate control is likely to be somewhat erratic, it is useful to develop a means to estimate the effects of rate variation on the data.

Figure 1c is a reprint of Figure 16 from *Tensile and Compression Mechanical Properties of Billet Pressed PBX 9502 as a Function of Temperature and Strain Rate*, Cunningham, Andreski, and Harwood, May 2003. The data demonstrates ordered relationships between strain rate, temperature, and ultimate tensile stress over a wide range of rates and temperatures. Assuming a similar ordering pattern for 900-24 data, which, like PBX 9502 is a composite containing Kel-F 800™ binder, we may construct a means to predict, approximately, the effect of rate changes on the ultimate strength of this material. This affords us the ability to understand sensitivities to, and potentially to correct for, deviations from a target rate.

In the tests performed in this 900-24 tensile matrix, tests were limited to just two nominal rates - 0.0001/s and 0.1/s. Lacking interim rate data we will make a simplifying assumption that ultimate stress varies linearly between, and in the region of these rate points. An examination of Figure 1c suggests that curvature is more than likely present, but that an assumption of linearity should provide a reasonable approximation.

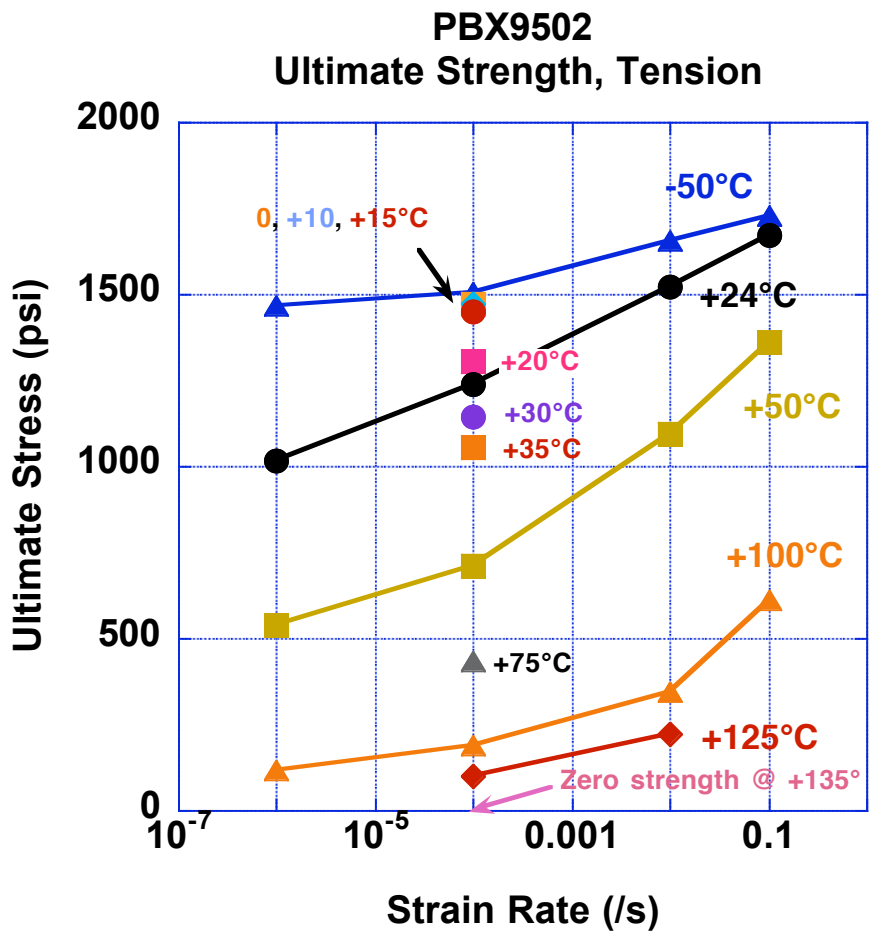

Figure 1c – PBX 9502 data illustrating strain-rate effects on ultimate tensile stress at constant temperature.

Using the test data generated in this series, we may construct the plots seen in Figure 2c. The curves shown can be expressed mathematically in the form:

$$ULT.STRESS_{RATE_2} = ULT.STRESS_{RATE_1} + A * Log_{10}[RATE_2 / RATE_1] \quad (1)$$

Where 'A' is a parameter determined from the data. From Figure 2, the three equations are:

$$ULT.STRESS(@-54^{\circ}C)_{RATE_2} = ULT.STRESS_{RATE_1} + 32 * Log_{10}[RATE_2 / RATE_1] \quad (2)$$

$$ULT.STRESS(@+24^{\circ}C)_{RATE_2} = ULT.STRESS_{RATE_1} + 74 * Log_{10}[RATE_2 / RATE_1] \quad (3)$$

$$ULT.STRESS(@+74^{\circ}C)_{RATE_2} = ULT.STRESS_{RATE_1} + 112 * Log_{10}[RATE_2 / RATE_1] \quad (4)$$

Collectively, these equations reflect, approximately, the material's ultimate stress sensitivity to rate over a range of temperatures and strain rates. Looking at the data specifically, we note that, on a percentage basis, the data that is most sensitive to rate control errors is the data at 74˚C.

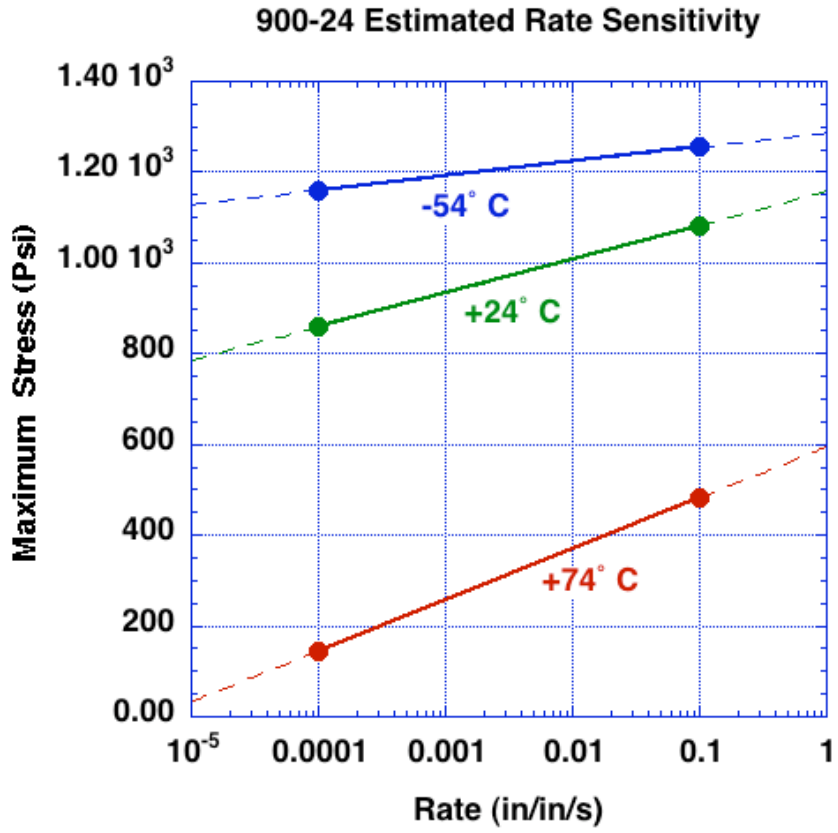

Figure 2c – The approximate rate sensitivity of mock 900-24 by temperature.

Typically, rate control is within a few percent of the target rate for slower rate tests. Occasionally, slippage in the actuating train or some other disturbance may cause a greater than usual rate control error. Examining the data for this series, we see that at 74˚C, there is a worst-case rate control error of about 3%. From equation 4, the estimate of difference in maximum stress for a 3% difference in rate control, relative to the target, is 1% at 74˚C. Looking at the data overall, we note that, as a worst case at the slow rate, we see an outlier at -54˚C where the actual rate was 0.087/s instead of 0.1/s.

This represents an error of approximately 13%. From equation 2, the estimate of error in ultimate stress is less than 0.2%.

At higher rates, rate control becomes much more difficult (see previous text). Excluding a single, exceptionally erroneous rate (see below), the average rate error is approximately 16%. To provide perspective, a 16% rate error, relative to the nominal high rate at 74˚C, would be expected to produce an error in ultimate stress of about 1.5%. At -54˚C, the error level would fall to under 0.2%.

We have included in the data set, a test that, on analysis, was found to have been conducted at a rate 5 times the nominal (0.5 vs. 0.1/s). This was test 4E from Hemi 4 performed at 74˚C. Looking at the plot for this test, it can be seen that the ultimate stress is quite high, relative to the other 04 hemi data in the group. From equation 4, a difference in rate of this magnitude would be expected to produce a difference in ultimate stress of approximately 16%, or about 80-psi. Looking at the plots in Figure 13, adjusting for the rate difference drops the ultimate stress from approximately 600-psi to roughly 520-psi, which is much more consistent with the other tests results.

Appendix D

SEM Images of Talc From Three Sources

At LLNL, we have found that the type of talc particles used in mock formulations appears to significantly influence the mechanical property behavior of insensitive HE mocks. In a report titled *Development of a Replacement Mock for the Insensitive High Explosives LX-17 and PBX 9502*, UCRL-JRNL-223040, July 2006, D. Mark Hoffman, B. Cunningham et al. found that talc with needle-like particles and a relatively greater particle size distribution appeared to produce notably stronger mocks than did a similar formulation with more spherical and uniformly-sized particles. Figure 10 in Hoffman's report highlights the difference in strength.

Figures 1d and 2d show SEM images of two talcs with different particle shapes. Figure 3d shows an image of talc particles extracted from the pressed 900-24 tensile sample that had arrived broken.

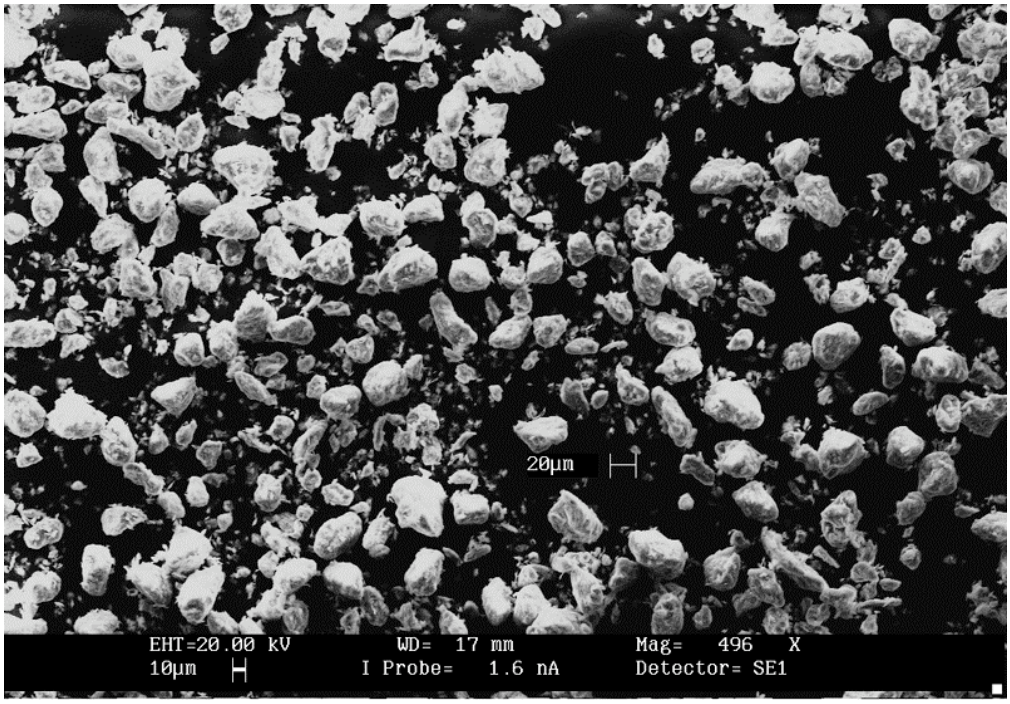

Figure 1d – Rounded particle, relatively uniform-sized talc, Silverline 202.

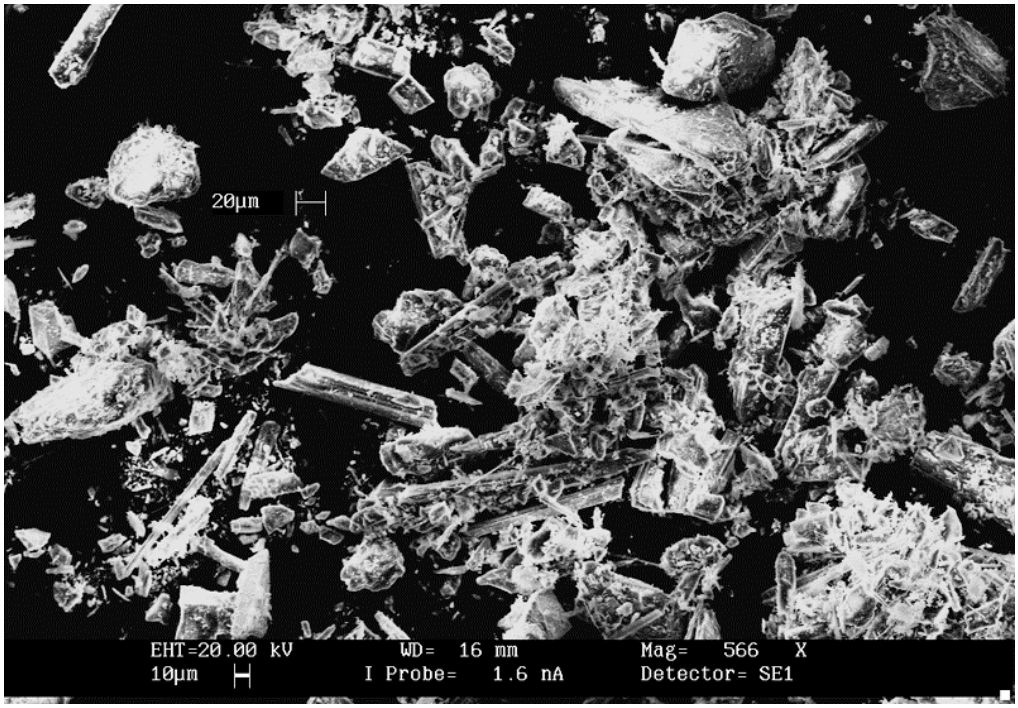

Figure 2d – Mixed size talc with needle-like particles, Nytal 99.

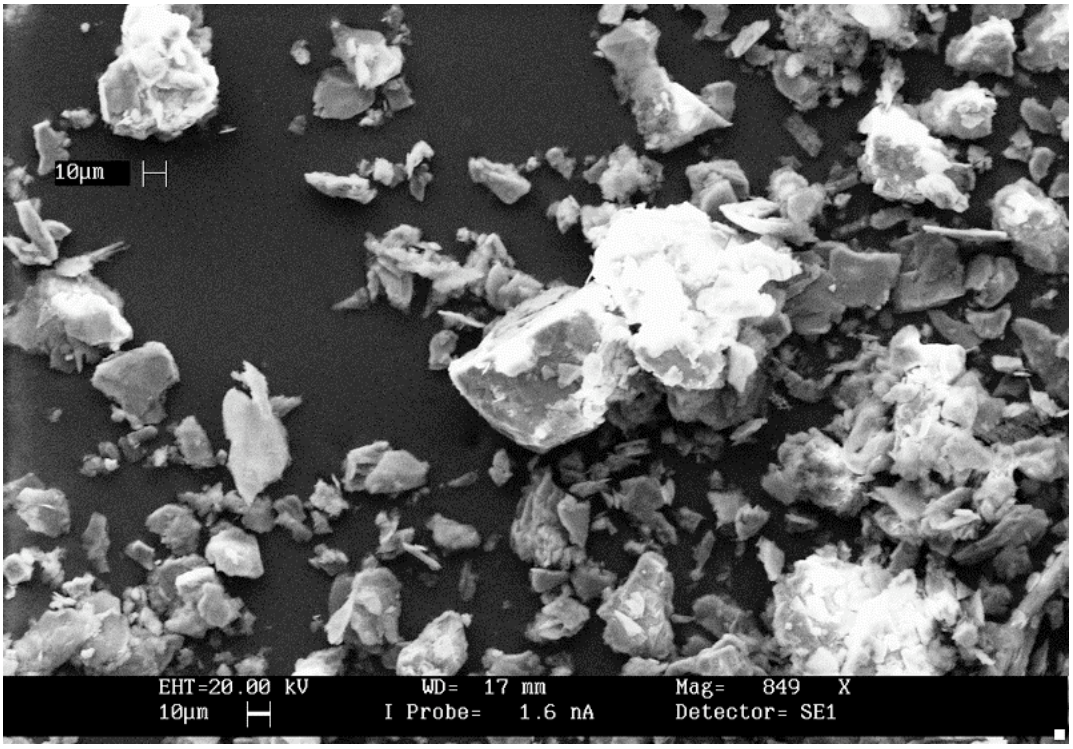

Figure 3d – Talc extracted from 900-24 pressed material. Particles are mixed size with no needle-like particles.

Appendix E

Effects of Pressing Temperature on 900-24 Performance

At our request, LANL provided us with 100 grams of 900-24 molding powder (lot #260-014) of the type used to produce the tensile samples tested in this study. Since, currently, we must create tensile specimens by machining them from billet or hemispherical pressings, we opted to conduct our sub-study using die-pressed compression specimens. In this very brief study, 0.5-inch diameter x 1.0-inch long compression specimens were pressed to a fixed volume using a standard 0.5-inch diameter precision die, fitted with coils that circulate heated oil. Five samples were pressed using shim stops and fixed amounts of powder to produce parts that were approximately the same density. Parts were pressed at room temperature, 80˚C, 90˚C (two), and 105˚C. These parts were then tested in compression at 24˚C at a rate of 0.0001/s – see Figure 1e.

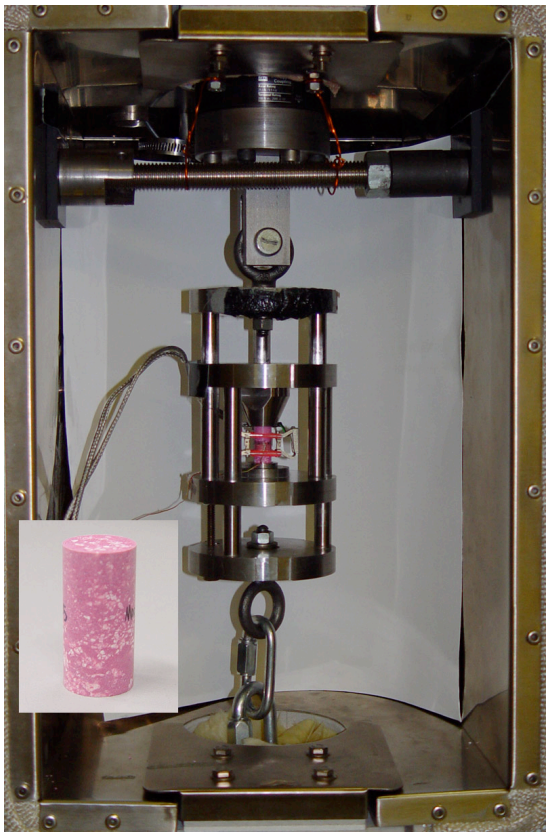

Figure 1e – Compression fixture with 0.5-inch diameter by 1-inch long cylindrical mock sample. A picture of a typical compression sample is inset.

Examining the data (see Figure 2e), we note that the part pressed at room temperature produced a smooth stress-strain curve but had very little

strength. Also, because of the elasticity of the unheated material, the density (1.765 g/cc) of this part was much lower than the other specimens, and noticeably below the target of 1.885-1.895 g/cc. The specimen pressed at 80˚C (1.887 g/cc) showed smooth loading throughout most of the test, but

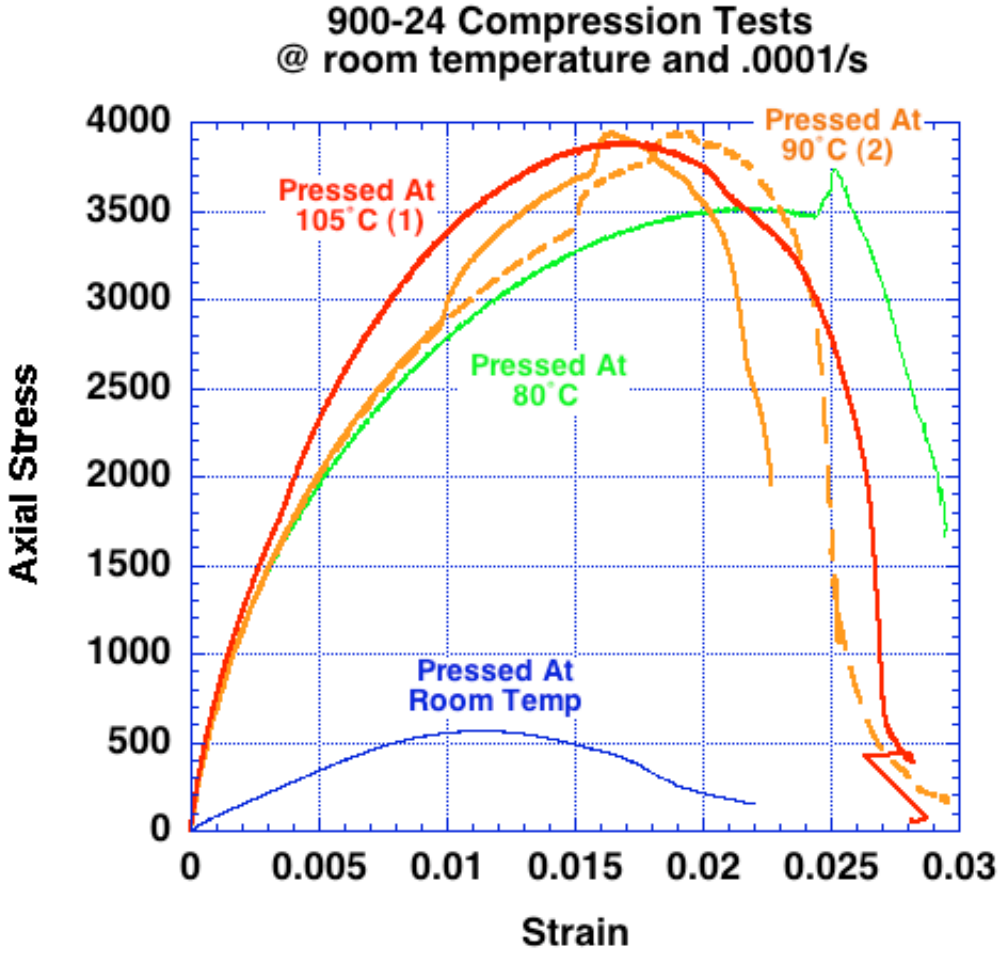

Figure 2e – Compression tests results from die-pressed mock 900-24 pressed at room temperature, 80˚C, 90˚C and 105˚C.

showed somewhat less strength at peak than was shown in the tests that followed. The two specimens pressed at 90˚C (1.879 and 1.883 g/cc) both exhibited good peak strength but also showed several instances during the tests where localized failure occurred – notice the curve discontinuities. Finally, the specimen pressed at 105˚C (1.887 g/cc) exhibited peak strength equivalent to that shown by the samples pressed at 90˚C, but showed little sign of discontinuities.

Compression tests of IHEs and mock IHEs are inherently different from tensile tests in that localized failure sites in compression tests tend to be "self healing". As stress increases, shear damage accumulates but the damage that occurs tends not to be catastrophic, since the nature of the loading is such that fractures will close as they develop. Failure eventually occurs due to an overwhelming accumulation of damage. In tension, however, failure occurs catastrophically (and at much lower levels of averaged strain) when a fracture propagates rapidly from a site of localized damage. Except at higher temperatures, there is little other damage to be found surrounding the fracture surface. Because this is true, material in tension is especially sensitive to the presence of flaws. We interpret the discontinuities that we see in the 90°C specimen compression curves to be evidence of the presence of flaws that could lead to tensile failure, had the specimens been subjected to tensile stress.